ACS APPLIED MATERIALS & INTERFACES

www.acsami.org

Research Article

Water-Repellent Perovskites Induced by a Blend of Organic Halide Salts for Efficient and Stable Solar Cells

Yuanyuan Zhang, Qiao Chen, Hyun-Seock Yang, Danbi Kim, Insoo Shin, Bo Ram Lee, Joo Hyun Kim, Doo Kyung Moon, Kwang Ho Kim,* and Sung Heum Park*

Cite This: *ACS Appl. Mater. Interfaces* 2021, 13, 33172−33181

Read Online

ACCESS | Metrics & More | Article Recommendations | Supporting Information

ABSTRACT: Despite tremendous progress in the power conversion efficiency (PCE) of perovskite solar cells (PeSCs), the long-term stability issue remains a significant challenge for commercialization. In this study, by blending organic halide salts, phenylethylammonium halide (PEAX, X = I, Br), with $CH_3NH_3PbI_3$ ($MAPbI_3$), we achieved remarkable enhancements in the water-repellency of perovskite films and long-term stability of PeSCs, together with enhanced PCE. The hydrophobic aromatic PEA^+ group in PEAX protects the perovskite film from destruction by water. In addition, the smaller halide Br^- in PEABr restructures $MAPbI_3$ to form $MAPbI_{3-x}Br_x$ during post-annealing, leading to lattice contraction with beneficial crystallization quality. The perovskite films modified by PEAX exhibited excellent water resistance. When the perovskite films were directly immersed in water, no obvious decompositions were observed, even after 60 s. The PEAX-decorated PeSCs exhibited considerable long-term stability. Under high-humidity conditions (60 ± 5%), the PEAX-decorated PeSCs held 80.5% for PEAI and 85.2% for PEABr of their original PCE after exposure for 100 h, whereas the pristine PeSC device lost more than 99% of its initial PCE after exposure for 60 h under the same conditions. Moreover, compared to the pristine device with a PCE of 13.28%, the PEAX-decorated PeSCs exhibited enhanced PCEs of 17.33% for the PEAI device and 17.18% for the PEABr device.

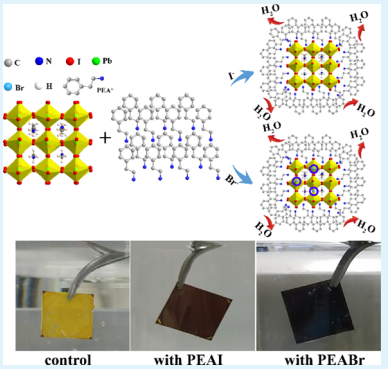

KEYWORDS: *phenylethylammonium halide, additive, water resistance, long-term stability, perovskite solar cells*

1. INTRODUCTION

Hybrid organic−inorganic perovskite solar cells (PeSCs) have achieved a satisfactory breakthrough in power conversion efficiency (PCE).[1−3] To date, their certified efficiency has exceeded 25%,[4] which makes them promising candidates for use in next-generation photovoltaics.[5,6] Despite their great success in efficiency improvement, PeSCs still suffer from severe instability toward heat, light, oxygen, and moisture, which largely prevents the commercialization of perovskite-based optoelectronic devices.[7−9] Among the influencing factors, moisture is considered the most prominent factor in the degradation of perovskite materials owing to the strong interactions of perovskites with water molecules.[10,11] In humid environments, perovskite materials, such as $CH_3NH_3PbI_3$, will degrade to CH_3NH_2, HI, and PbI_2, thereby losing their photoelectric conversion properties.[3,12,13]

Over the past several years, the use of additive materials has made significant contributions to improving the moisture stability of PeSCs together with their PCEs.[14−16] The introduction of effective additives, including inorganic nanocrystals, fullerene, polymers, metal halides, small organic molecules, and organic halide salts, has altered the morphology and crystallinity of the perovskite films while improving the optical and electrical characteristics of the perovskite active layers. Yang et al.[17] achieved enlarged perovskite grains. The defect density decreased by incorporating dimethyl itaconate into the PbI_2 solution for highly efficient PeSCs with long-term stability. Xie et al.[18] utilized (3-mercaptopropyl)-trimethoxysilane to passivate defects via a Lewis acid−base interaction with PbI_2. They also achieved enhancements in the PCE and long-term stability with larger grain sizes and longer carrier lifetimes.

Recently, long organic cations have been considered promising additives to enhance the stability of perovskite crystals.[19−21] In particular, phenyl ethylammonium halides (PEAX, X = I or Br) are widely used as organic cations.[22,23] Zhou et al.[24] used a PEAI additive to obtain 2D/3D mixed perovskites with modulated diffusion passivation and improved device efficiency and stability. In addition, Liu et al.[25] treated the perovskite top surface with phenyl ethylammonium halide, thereby improving the PCE and thermal stability of PeSCs by obtaining a quasi-2D PEA_2PbI_4 perovskite. You et al.[4] utilized a PEAI passivation layer to reduce the number of defect sites and

Received: May 18, 2021
Accepted: June 29, 2021
Published: July 9, 2021

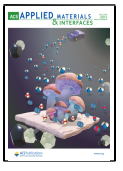

https://doi.org/10.1021/acsami.1c09093
ACS Appl. Mater. Interfaces 2021, 13, 33172−33181

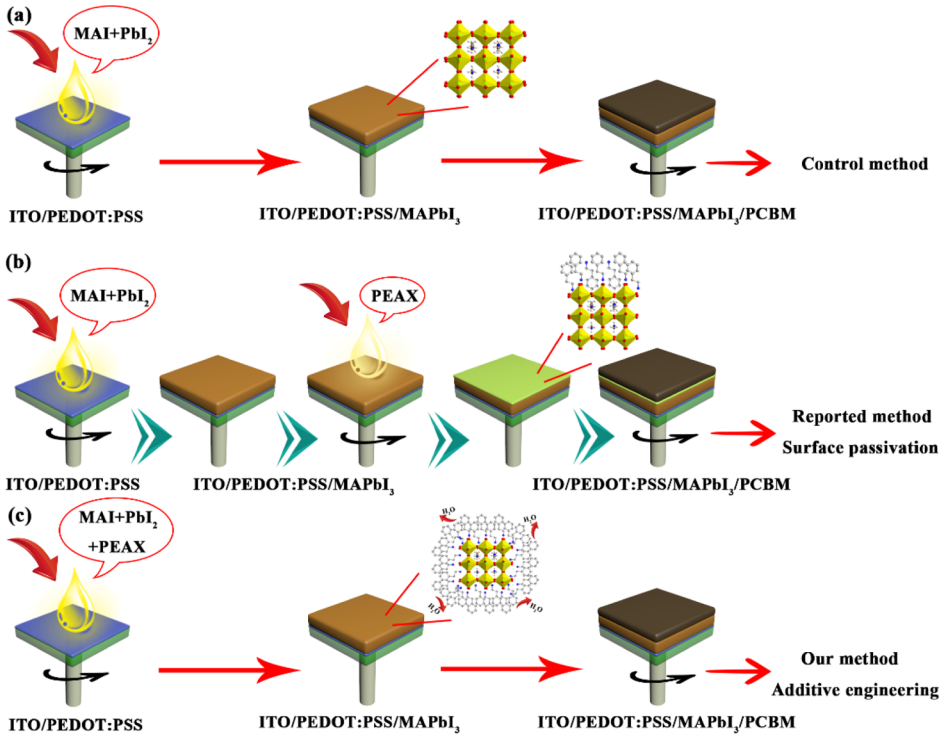

Figure 1. Schematics of PEAI-induced film fabrication processes: (a) control method, (b) reported surface passivation method, and (c) developed additive engineering.

suppress nonradiative recombination, resulting in an improved certified efficiency of 23.32%. More recently, Liu et al.[26] treated the surface of a perovskite film with phenylethylammonium chlorine (PEACl) and PEABr to improve the humidity resistance of inorganic perovskite materials. They contended that PEACl and PEABr played important roles in the formation of a hydrophobic layer on the perovskite surface and controlled the crystallization and lattice shrinkage of the perovskite film induced by the doping effect of Cl^- and Br^-.

Despite the advantages of surface treatment with PEAX for enhancing the PCE and stability, additional steps are inevitably required in device fabrication for the PEAX additive deposition. Moreover, most researchers have focused on the utilization of PEAX as a surface passivation material to improve the humidity resistance of perovskite films.[4,26] Accordingly, PEAX was mainly coated on the top of the perovskite layer after perovskite active layer deposition. Although the passivating effect of the deposition of the PEAX layer on the top of the perovskite active layer was available, the top passivating layer hardly protected the perovskite crystal owing to the imperfect shielding and nonideal water resistance of the perovskite itself.

In this study, we developed a simple and highly effective passivating method for perovskite active layers for highly efficient and stable PeSCs. By dissolving PEAX (X = I, Br) directly into the $MAPbI_3$ precursor solution, we achieved remarkably enhanced water resistance of the perovskite films. The hydrophobic aromatic group PEA^+ in PEAX protects the perovskite from destruction by water. In addition, the smaller halide Br^- in PEABr participates in the restructuring of the lattice of $MAPbI_3$ to form $MAPbI_{3-x}Br_x$ during post-annealing, causing a smaller lattice structure with a beneficial crystallization quality. As expected, the objective films exhibited excellent stability under an ambient environment with a relative humidity (RH) of 60 ± 5%, and no obvious decomposition was observed after being directly soaked in water for 60 s. Meanwhile, the PEAX-treated devices presented long-term stability with more than 76.5 and 82.8% of the initial PCE for PEAI and PEABr over 500 h under an ambient environment with a RH of 30 ± 5%, respectively, which is much higher than that (25.6%) of the control device. Even under high-humidity conditions (60 ± 5%), PeSCs modified by PEAI and PEABr still held 80.5 and 85.2% of the original PCE after 100 h, respectively. In contrast, the pristine PeSC device lost over 99% of its initial PCE after only 60 h under the same conditions. In addition, compared to the pristine device with a PCE of 13.28%, the PEAX-decorated PeSCs exhibited enhanced PCEs of 17.33% for the PEAI device and 17.18% for the PEABr device.

2. EXPERIMENTAL SECTION

2.1. Material Preparation. Methylammonium iodide (CH_3NH_3I, MAI) and lead iodide (PbI_2) were obtained from Tokyo Chemical Industry. PEAI and PEABr were purchased from GreatCell Solar. All solvents including dimethyl formamide (DMF), dimethyl sulfoxide (DMSO), and chlorobenzene (CB) were bought from Sigma-Aldrich. The $MAPbI_3$ precursor solution with concentration of 1.1 mol/L was prepared by dissolving MAI and PbI_2 [MAI (n)/PbI_2 (n) = 1:1] in a mixed solvent [DMF (v)/DMSO (v) = 10:1]. For the phenyl ethylammonium halide-modified precursor solutions, we directly dissolved PEAI or PEABr into the $MAPbI_3$ solution. The concentrations of PEAI and PEABr were 1, 3, 5, and 10 mg/mL. A 30 mg/mL 6,6-phenyl-C_{61}-butyric acid methyl ester (PCBM) solution was used as the electron transport layer.

2.2. Device Fabrication. The experiment was performed according to our previous work.[27] In a typical process, the poly(3,4-ethylenedioxythiophene):poly(styrene sulfonate) (PEDOT:PSS) solution was first deposited on cleaned indium tin oxide (ITO) glass at 4500 rpm for 40 s and then heated at 145 °C for 20 min. Subsequently, the ITO glass was transferred to a glovebox and cooled to room temperature. A perovskite precursor solution without or with PEAX was spin-coated on the PEDOT:PSS film at 1200 rpm for 5 s and then at

https://doi.org/10.1021/acsami.1c09093
ACS Appl. Mater. Interfaces 2021, 13, 33172−33181

4500 rpm for 50 s. After starting at the second step for 5 s, 200 μL of CB was used as an anti-solvent to wash the perovskite film. Then, the PCBM solution was spin-coated onto the perovskite layer at 1500 rpm for 30 s. Next, the ITO glass was annealed at 120 °C for 10 min in a vacuum oven at a low pressure of -8×10^4 Pa. From that point, the PCBM film was eliminated by rinsing with CB, and a new PCBM layer was re-spin-coated on the perovskite layer. Finally, a complete device was obtained by evaporating the Al electrode on the film.

For the reported surface passivation strategy, PEAI or PEABr solution with a concentration of 5 mg/mL was deposited on top of the annealed $MAPbI_3$ film. The other procedures were the same as those used for the control device.

2.3. First-Principles Calculations. First-principles calculations were performed using the well-tested Cambridge Serial Total Energy Package code based on density functional theory.[28−30] To obtain the ideal results, a super cell ($2 \times 2 \times 2$, total I atom number of 96) of $MAPbI_3$ was constructed. For $MAPbI_{3-x}Br_x$, three I atoms were replaced by Br to calculate the band structure and density of states. A fixed cutoff energy of 380 eV was set as the Vanderbilt ultrasoft pseudopotential. Brillouin zone integration was represented by adopting the *K*-point sampling scheme of $4 \times 4 \times 2$ Monkhorst−Pack grids. Geometry optimization was performed using the Broyden, Shannon, Fletcher, and Goldfarb routes and the positions of all atoms were simultaneously optimized during the geometry optimization process. The convergence criterion for geometry optimization was chosen with the differences in the total energy (5.0×10^{-6} eV/atom), a maximal ionic Hellmann−Feynman force of 0.01 eV/Å, a stress tensor of 0.02 GPa, and the maximal displacement of 5.0×10^{-4} Å. The exchange and correlation functions within the generalized gradient approximations in accordance with the Perdew−Burke−Ernzerhof scheme were used to perform the calculation.

3. RESULTS AND DISCUSSION

Figure 1 shows the three types of fabrication methods. Figure 1a depicts the conventional fabrication method for the perovskite active layer without PEAX treatment. In this method, the MAI and PbI_2 solutions are spin-coated on the PEDOT:PSS layer, and then the PCBM layer is deposited on the perovskite layer. Figure 1b shows the coating method for the surface passivation with PEAX. Compared to the conventional method shown in Figure 1a, PEAX is spin-coated on the perovskite layer before deposition of the PCBM layer in this method. In this case, an additional step for the PEAX coating is required. Figure 1c presents our PEAX blend method for the perovskite active layer. After blending the PEAX with the perovskite precursor in solution, the perovskite blend solution was coated onto the PEDOT:PSS layer. Except for the use of the blend of PEAX and perovskite precursor instead of a single perovskite precursor, this fabrication process is exactly the same as the conventional method in Figure 1a, and it is simpler than the coating method in Figure 1b because it has no additional steps.

The effect of PEAI on the crystal structure and morphology of the perovskite film was investigated first. Since the PEAX coating method with an additional coating step (Figure 1b) was already studied in our earlier works,[31] we focused on the analysis of the films prepared by the PEAX blending method, as shown in Figure 1c. Figure 2a presents the X-ray diffraction (XRD) patterns of the perovskite films with different concentrations of PEAI. For pristine perovskite with a concentration of 0 mg/mL (red color), weak diffraction peaks of $MAPbI_3$ corresponding to diffraction peaks of intermediate phases ($MAI{\cdot}PbI_2{\cdot}DMF$) are observed.[32] The peaks of the intermediate phases marked by the symbol ▼ apparently decrease when 1 mg/mL of PEAI is added to the perovskite precursor solution. As the content of PEAI continually increases (3−10 mg/mL), the peaks of intermediate phases disappear. Only the $MAPbI_3$ signals were monitored and

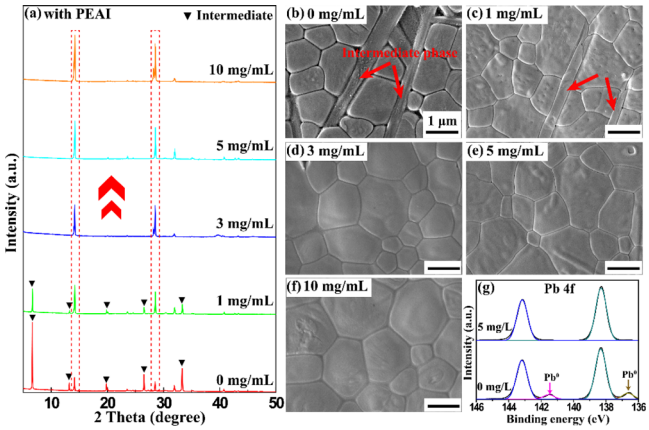

Figure 2. (a) XRD patterns of perovskite films with different concentrations of PEAI. (b−f) SEM images of perovskite films with different concentrations of PEAI. (g) High-resolution XPS spectra of Pb 4f level.

indicated the complete conversion of the intermediate phase into perovskite. In addition, the main peak intensity of $MAPbI_3$ strengthened with an increase in the PEAI concentration. These results indicate that PEAI can accelerate the conversion of intermediates and strengthen the crystallization of perovskite, which is intuitively reflected by scanning electron microscopy (SEM) images.

As shown in Figure 2b,c, both intermediate rods[33] and perovskite grains are clearly observed in the $MAPbI_3$ films with PEAI with concentrations of 0 and 1 mg/mL. Interestingly, when the PEAI concentration increases, the rod-like intermediates vanish; only perovskite grains are observed (Figure 2d−f). This finding implies the complete conversion of intermediates, which is consistent with the XRD analysis shown in Figure 2a. In addition, the SEM images (Figure 2d−f), the elemental mappings (Figure S1), and the cross-sectional SEM images (Figure S2a,b) indicate that a high-quality perovskite film with a uniform and pinhole-free surface can be obtained by simply blending PEAI with a perovskite precursor.

The effect of PEAI on the accelerated conversion of intermediates was also identified via X-ray photoelectron spectroscopy (XPS). As shown in Figure 2g, the Pb 4f level of pristine perovskite presents four peaks. The two peaks at the binding energies of 143.18 and 138.53 eV are attributed to Pb $4f_{5/2}$ and $4f_{7/2}$, respectively, which is aligned with the values reported for Pb interacting with I^-.[34] The other two shoulder peaks at the binding energies of 141.53 and 136.64 eV are assigned to Pb^0.[35] However, for the PEAI-decorated perovskite film, the peaks of Pb^0 are successfully inhibited, indicating the complete conversion of intermediates into perovskite.

These trends were also observed in the perovskite films prepared with the perovskite precursor blended with PEABr in solution. When we performed the same experiments for the films with PEABr, we obtained almost the same results as those of the PEAI film. The results of the cross-sectional SEM image (Figure S2c), XRD patterns in Figure S3, and top view of the SEM images in Figure S4 are consistent with those of PEAI, which also confirms the accelerated intermediate conversion by PEABr. Moreover, the 2θ value of the (110) plane of the PEABr-modified perovskite film shows a slight shift toward a higher value than that of pristine $MAPbI_3$ (Figure S5). Based on previous studies, the enlarged diffraction angle could be attributed to the reduced lattice spacing.[36] Because the radius

https://doi.org/10.1021/acsami.1c09093
ACS Appl. Mater. Interfaces 2021, 13, 33172−33181

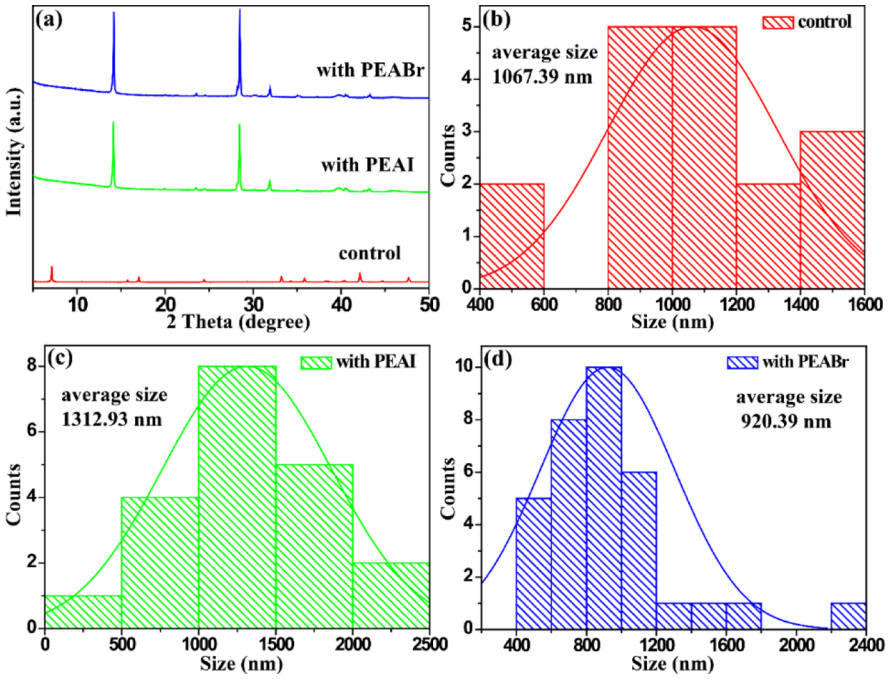

Figure 3. (a) XRD patterns of different perovskite films. (b–d) Grain size distributions of perovskite films.

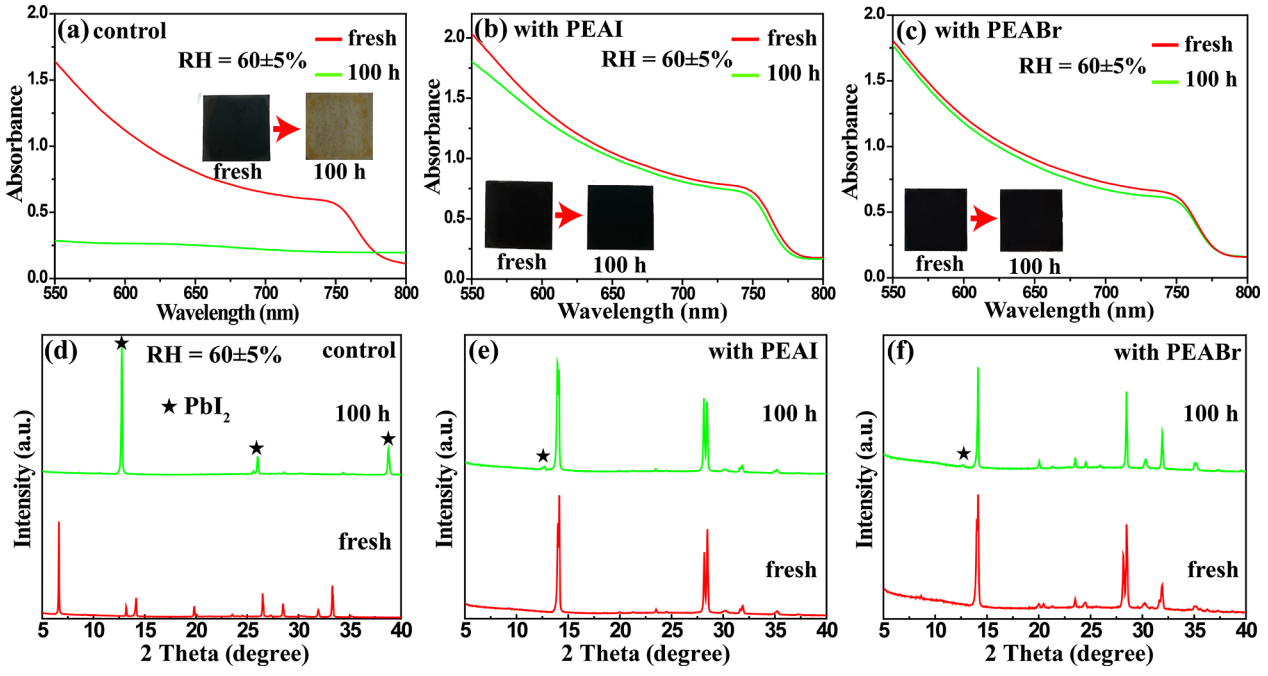

Figure 4. Changes of ultraviolet–visible absorption spectra and film colors for () control film, (b) PEAI-treated film, and (c) PEABr-treated film under a RH of 60 ± 5%. The XRD pattern evolution of the (d) control film, (e) PEAI-treated film, and (f) PEABr-treated film under a RH of 60 ± 5% for 100 h.

of Br^- (0.195 nm) is smaller than that (0.216 nm) of I^-, it is reasonable to infer that Br^- participates in the lattice restructuring of $MAPbI_3$ to form $MAPbI_{3-x}Br_x$. The high-resolution Br 3d XPS spectrum (Figure S6) and elemental distributions (Figure S7) suggest the existence of Br in the perovskite film, confirming the doping of Br^- into the lattice of $MAPbI_3$.

The introduction of Br^- could cause lattice strain and enhance the crystallization of $MAPbI_3$, as demonstrated by the XRD patterns and size distribution images. As shown in Figure 3a, the PEABr-treated perovskite film presents stronger diffraction peaks compared to that of the PEAI-modified perovskite. In addition, the average grain size calculated by the analysis software of "Nano Measure" for PEABr film is much smaller than those of the control and PEAI-modified perovskite films (Figure 3b–d). These results suggest that the doping of Br^- could induce lattice shrinkage and improve the crystallization of perovskite, which contributed to the enhanced moisture resistance (confirmed by Figure S8).

https://doi.org/10.1021/acsami.1c09093
ACS Appl. Mater. Interfaces 2021, 13, 33172–33181

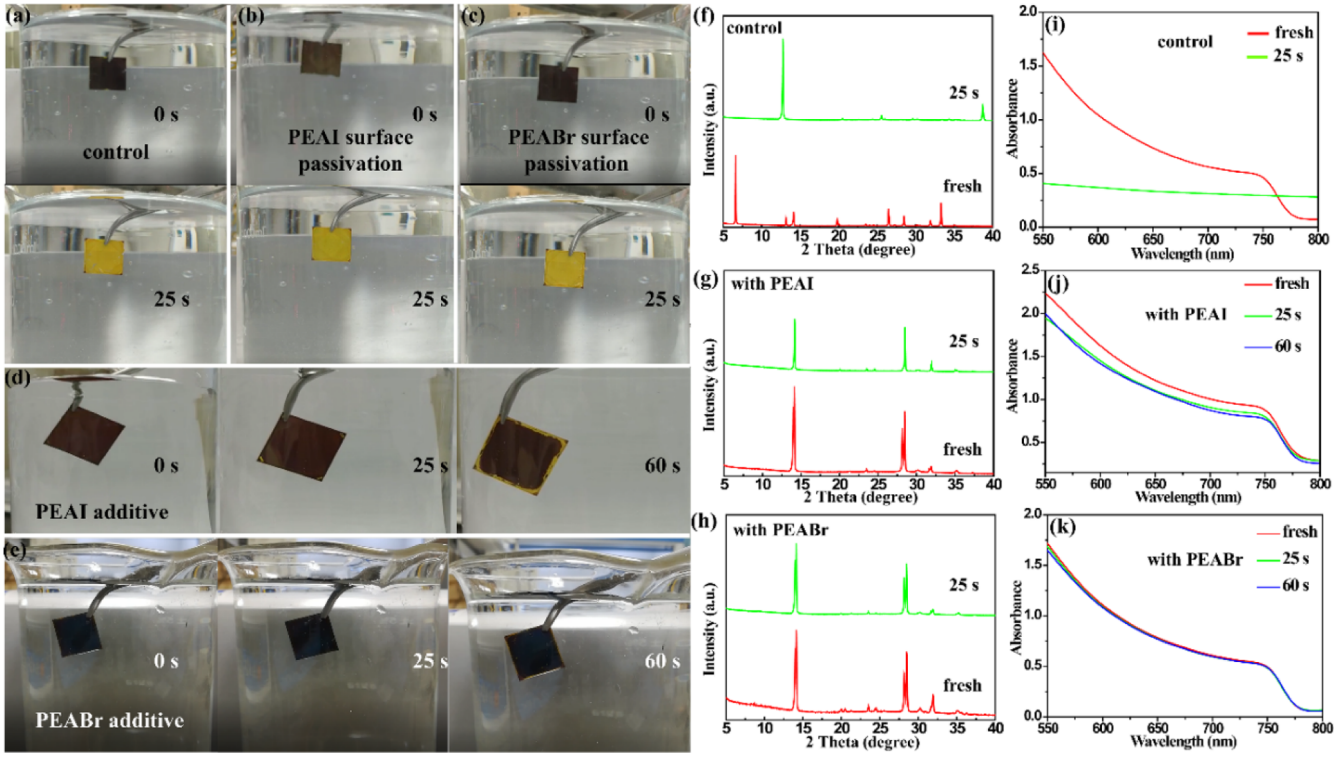

Figure 5. (a–e) Photographs of the color changes of the modified and nonmodified perovskite/PCBM films immersed in water as a function of time. (f–h) XRD patterns and (i–k) ultraviolet–visible absorption spectra of modified and nonmodified perovskite/PCBM films after immersing in water.

The use of PEAX (X = I, Br) is expected to improve the water resistance of perovskite films by forming a hydrophobic capping layer.[37,38] As shown in Figure S8, the perovskite film with PEAX exhibits a larger contact angle than that of the pure $MAPbI_3$ layer, implying enhanced moisture resistance by PEA^+. Moreover, the lattice contraction and strengthened crystallization of perovskite induced by the doping of Br^- could further improve the moisture resistance, which is confirmed by the larger contact angle of the PEABr-treated film than that of the PEAI-treated film.

To further confirm the enhanced stability of the PEAX-modified perovskite film, we first investigated the moisture resistance of the perovskite film under a RH of 60 ± 5%. Figure 4a presents the UV–visible absorption spectra of the perovskite films with and without PEAX. After exposure for 100 h, the absorption intensity of the control film is dramatically reduced, which is ascribed to the perovskite decomposition into intermediates and PbI_2.[39] This reduction is intuitively reflected by the color changes of the perovskite films. As shown in Figure S9, the color of the control film slightly changes to yellow after storage for 5 h, and then it completely converts to yellow after 100 h of exposure (insets of Figure 4a). In contrast, the perovskite films with PEAX nearly maintain their initial absorbance at the same time (see Figure 4b for the PEAI film and 4c for the PEABr film). As expected, the colors of the PEAX-decorated films retain their initial colors even after exposure for 100 h. Furthermore, the XRD patterns of the perovskite films can also confirm the stability performance in humid environments. Compared to the control film in Figure 4d, the diffraction peaks of the PEAX-treated perovskite films in Figure 4e,f are almost unchanged after exposure for 100 h. However, only the peaks of PbI_2 can be detected for the control film after the same time, suggesting the complete decomposition of perovskite and intermediates to PbI_2. These results imply that the excellent stability of the perovskite layer in a humid environment can be realized by the modification of PEAX.

To further demonstrate the strong stability of films induced by PEAX, we directly immersed the perovskite/PCBM films in water and compared their color changes to each film as a function of time (see Movie S1). When a pristine perovskite/PCBM film was soaked in water, it decomposed immediately with a rapid color change from black to yellow. It is easily understood that water molecules permeate into the perovskite layers and destroy their crystal structures. After immersion for approximately 25 s, the color of the pristine film completely converted to yellow (Figure 5a). This trend was also observed in the films with the surface coating of PEAX, as described in Figure 1b. As depicted in Figure 5b,c, the colors of the perovskite films also change quickly after immersion in water, indicating the weak water resistance of the films. In contrast to these films, the film fabricated by our blending method described in Figure 1c exhibited strong resistance to water with no noticeable color change after soaking for 25 s (see Figure 5d,e). Even after water immersion for 60 s, only the edge of the PEAI-treated film slightly changed to yellow, while the majority of films still maintained a black color. The XRD data also confirm the excellent stability of the PEAX-modified perovskite films after immersion. While the pristine perovskite in Figure 5f completely degrades to PbI_2 with enlarged peak intensity after soaking for 25 s, the PEAX-treated films in Figure 5g,h nearly retain their initial peak intensity. Ultraviolet–visible absorption spectra also confirmed the enhanced water resistance of the films by PEAX. As depicted in Figure 5i–k, nearly no absorption is observed for the pure film after immersion for 25 s owing to the complete degradation of perovskite to PbI_2. Conversely, PEAX-decorated films show only a slight decrease after soaking for 25 or 60 s, suggesting that PEAX-induced additive engineering could protect the perovskite film by resisting water.

https://doi.org/10.1021/acsami.1c09093
ACS Appl. Mater. Interfaces 2021, 13, 33172–33181

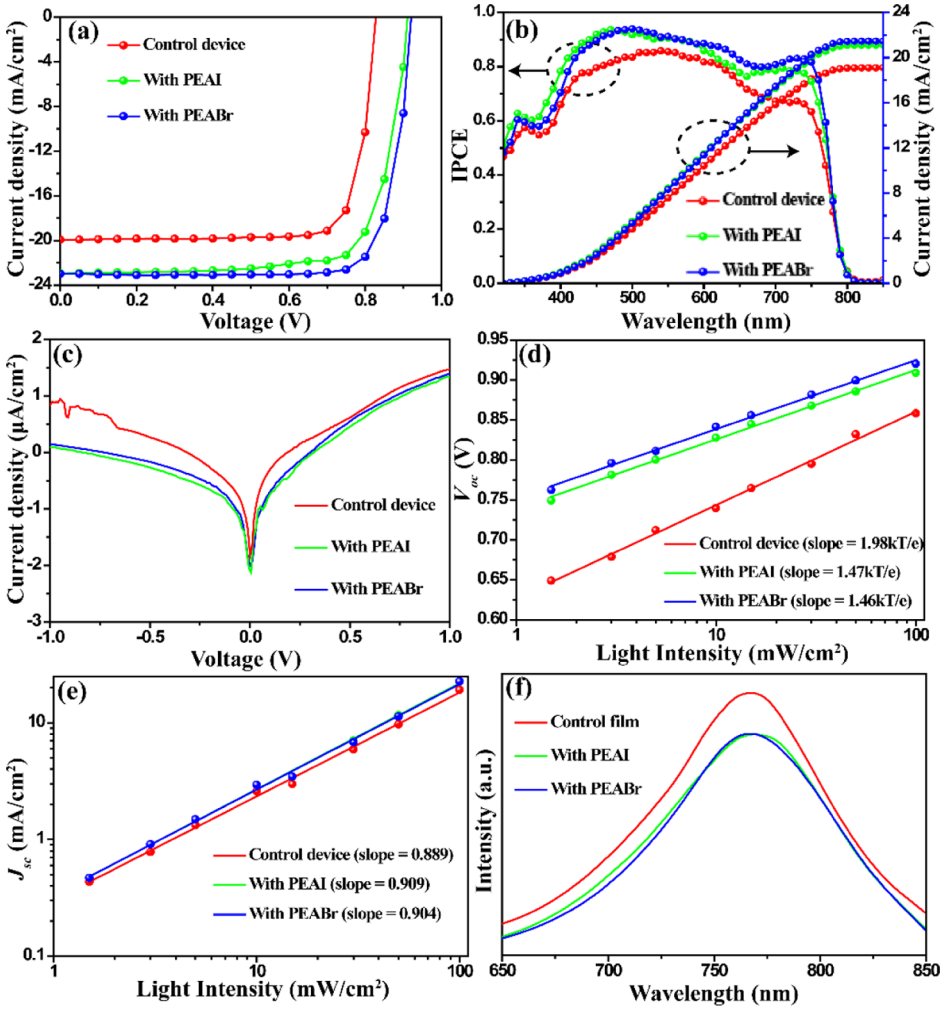

Figure 6. (a) $J-V$ curves and (b) IPCE spectra of the champion solar cell devices. Dependence of (c) J_{sc} and (d) V_{oc} on illumination intensity. (e) Dark current−voltage responses of the electron-only devices. (f) Steady-state PL spectra of perovskite films.

To study the effect of PEAX on the photovoltaic performance of the devices, we constructed inverted PeSCs with the architecture of ITO/PEDOT:PSS/perovskite (with or without PEAX)/PCBM/Al. The corresponding schematic structure is shown in Figure S10. Figure S11 presents the current density versus voltage ($J-V$) curves of the PeSCs constructed from different concentrations of PEAX under a standard AM 1.5 G irradiation of 100 mW/cm^2. The corresponding photovoltaic parameters are summarized in Tables S1 and S2. It can be clearly observed that the PCE of PeSCs initially improves and then decreases with the increase in the PEAX concentration. From Figure S11, 5 mg/mL was selected as the optimal concentration for PEAI and PEABr. Figure 6a shows the $J-V$ curves of the control and objective champion devices. The control device has a relatively low PCE of 13.28%, short-circuit current density (J_{sc}) of 19.77 mA/cm^2, open-circuit voltage (V_{oc}) of 0.84 V, and fill factor (FF) of 80.26%. After the treatment with PEAX, the champion device presents obviously improved photovoltaic characteristics, with PCE of 17.33%, J_{sc} of 22.95 mA/cm^2, V_{oc} of 0.91 V, and FF of 82.89% for PEAI and PCE of 17.18%, J_{sc} of 22.98 mA/cm^2, V_{oc} of 0.92 V, and FF of 81.19% for PEABr. For the PEAX-treated device, the enhanced efficiencies mainly originate from the increased J_{sc}, which is consistent with the improved incident photo-to-current efficiencies (IPCEs) over the entire wavelength region (Figure 6b). The enhanced IPCEs are sensitive to their high crystallinity and large grain size (confirmed by XRD and SEM analysis), resulting in reduced device resistance and a decreased number of grain boundaries on the charge carrier transfer pathway.[40] Moreover, as depicted in Figure 6c, the dark $J-V$ spectra of the PEAX-decorated devices with reduced leakage current indicate their higher shunt resistances, contributing to the increase in J_{sc}.[41,42]

Efficient charge carrier transfer is also an important factor for the enhancement of PCE of PeSCs.[43,44] The changes in J_{sc} and V_{oc} under various light intensities were studied to determine the charge migration characteristics of the PeSCs with and without PEAX modification.[12] Figure 6d shows the dependence of V_{oc} on the logarithm form of the incident light intensity $[\log(I)]$ according to the equation $V_{oc} = \varepsilon kT \ln(I)/e + \text{constant}$,[45] where ε is the ideal factor, k is the Boltzmann constant, T is the absolute temperature, and e is the elementary charge. The ε values are calculated to be 1.47 and 1.46 for the PeSCs treated by PEAI and PEABr, respectively, which are much smaller than that (1.98) of the control device. An ε value larger than 1 indicates the presence of supererogatory trap-assisted Shockley−Read−Hall (SRH) recombination, and a decreased ε value suggests a suppression of the monomolecular SRH recombination.[46,47] In addition, based on $J_{sc} \propto I^{\alpha}$, the dependence of J_{sc} on the logarithmic form of light intensity (I) is shown in Figure 6e. The slopes were determined to be 0.909 and 0.904 for the devices

https://doi.org/10.1021/acsami.1c09093
ACS Appl. Mater. Interfaces 2021, 13, 33172−33181

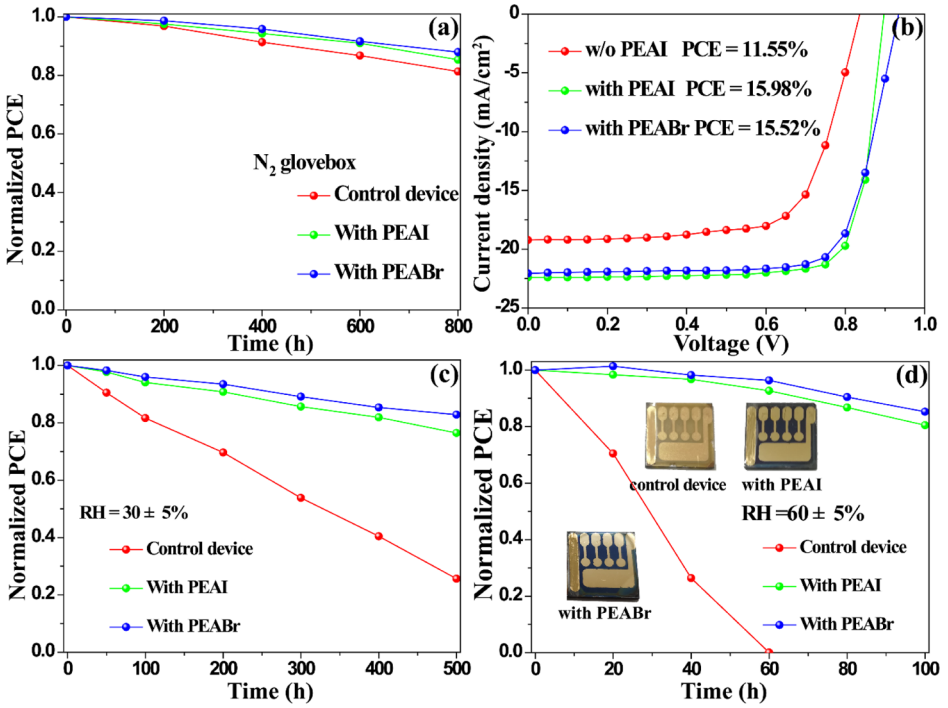

Figure 7. (a) Stability evolution of devices with the structure of the ITO/PEDOT:PSS/$MAPbI_3$/PCBM/Al electrode without encapsulation under a N_2-filled glovebox. (b) $J-V$ curves of devices. Stability evolution of the unencapsulated device with the structure of the ITO/PEDOT:PSS/$MAPbI_3$/PCBM/Au electrode under an ambient environment with a RH of (c) 30 ± 5 and (d) 60 ± 5%. The color changes of the three devices (inset of d).

modified with PEAI and PEABr, respectively, which are slightly larger than that (0.889) of the control device. The larger slope value implies the effective inhibition of bimolecular recombination during sweeping out the charge carriers at the interface of the perovskite film and charge-transfer layer.[48,49] Furthermore, in Figure 6f, an obvious quenching can be observed in the steady-state photoluminescence (PL) spectra of the PEAX-decorated perovskite films, indicating their efficient charge carrier transfer.[50]

In terms of the PEABr-modified device, except for the enhanced J_{sc} and efficient charge carrier transfer, the increase of the V_{oc} value is also a crucial factor to improve the PCE of PeSCs, which is sensitive to the energy-level position of the materials. Based on the analysis of Figures S5−S7, Br^- was successfully doped into the perovskite lattice. To study the influence of Br^- doping on the band structure of $MAPbI_3$, first-principles calculations based on the density functional theory method were conducted. According to the quantitative analysis from XPS in Table S3, the atomic ratio of I to Br is approximately 32:1. Because there are only 12 iodine atoms in one unit cell (Figure S12), a super cell (2 × 2 × 2, the total I atom number is 96) of $MAPbI_3$ was constructed (Figure S13), and three I atoms were replaced by Br to guarantee calculation precision. As shown in Figure S13, the two types of I^-, including I1 and I5 (the Wyckoff positions are 8d and 4c, respectively) can be found in the $MAPbI_3$ unit cell, and their atomic parameters are listed in Table S4. Figure S14 shows the crystalline structures of pure $MAPbI_3$ and $MAPbI_{3-x}Br_x$ with possible substitution positions, and their band structures and partial density of states were calculated. For the pristine $MAPbI_3$, its valence band maximum (VBM) and conduction band minimum (CBM) are mainly constituted by the I 5p and Pb 6p energy levels, respectively (Figure S14a). After introducing Br, a new Br 2p energy level is observed, which was hybridized with the I 5p level and became a part of the VBM (Figure S14b−e). As evident from the calculated band structures, all mixed halide hybrid perovskites $MAPbI_{3-x}Br_x$ exhibit larger band gaps compared with that of pure $MAPbI_3$.

Furthermore, the effect of Br^- substitution on the band structure of $MAPbI_3$ was investigated via ultraviolet photoelectron spectroscopy (UPS). Figure S15 shows the UPS spectra of the perovskite films. The work functions (Φ) of the perovskite films without and with PEABr are calculated to be 4.31 and 4.51 eV (vs vacuum), respectively, according to the equation $\Phi = 21.22 - E_{cutoff}$.[51] The distances between the VBM and Fermi level (E_f) are approximately 1.35 and 1.22 eV for the $MAPbI_3$ and $MAPbI_{3-x}Br_x$, respectively. Therefore, the corresponding VBM values are determined to be 5.66 and 5.73 eV for $MAPbI_3$ and $MAPbI_{3-x}Br_x$, respectively. Moreover, from the absorption spectra in Figure S16, the absorption edges of the $MAPbI_3$ and $MAPbI_{3-x}Br_x$ are 787 and 790 nm, respectively, with corresponding band gaps calculated as 1.57 and 1.58 eV, respectively. Based on the equation $E_g = E_{VBM} - E_{CBM}$,[52] the CBM values are calculated to be 4.09 and 4.51 eV for $MAPbI_3$ and $MAPbI_{3-x}Br_x$, respectively. These results suggest that Br^--induced lattice restructuring could control the band structure and enlarge the band gap of the mixed halide hybrid perovskite, leading to an enhanced V_{oc}, consistent with previous reports.[53,54]

The long-term stability of PeSCs is a crucial issue for realizing their commercialization.[55] Figure 7a depicts the PCE damping curves of the PeSCs under a N_2-filled glovebox without encapsulation. It can be observed that the PCEs of the three devices are reduced in accordance with an increase in storage time. Over 85% of the initial PCEs are held for PEAX-modified PeSCs after 800 h of exposure, which is slightly higher than that of the control device. This is because Al electrodes are easily vulnerable in humid environments, especially in contact with PCBM films (Figure S17).[56]

https://doi.org/10.1021/acsami.1c09093
ACS Appl. Mater. Interfaces 2021, 13, 33172−33181

To confirm the stability of the perovskite film decorated with PEAX additives, we used a Au electrode to replace Al and construct the PeSC devices. Although their PCEs were slightly lower than those of the device with the Al electrode (Figure 7b), long-term stability could be realized. As shown in Figure 7c, the PeSCs with PEAI and PEABr can maintain more than 76.5 and 82.8% of their original PCE in an ambient environment with a RH of 30 ± 5% over 500 h, which is much higher than that (25.6%) of the control device. Even when the humidity reaches 60 ± 5%, the PeSCs modified by PEAI and PEABr still hold 80.5 and 85.2% of the original PCE after exposure for 100 h, respectively (Figure 7d). However, the control device degrades rapidly, with a PCE loss of over 99% of the initial value after only 60 h. The color changes in the inset of Figure 7d can intuitively reflect the stability of the devices.

4. CONCLUSIONS

In summary, we successfully developed an effective strategy to improve the PCE and stability by mixing a PEAX additive into the perovskite precursor solution. The hydrophobic aromatic group PEA^+ as a capping layer could protect the perovskite from destruction by water. In addition, the smaller halide Br^- in PEABr could participate in the lattice restructuring of $MAPbI_3$ to form $MAPbI_{3-x}Br_x$ during post-annealing, leading to a smaller lattice structure with a beneficial crystallization quality. These variations contributed to improving the stability of the perovskite films. As expected, the PEAX-treated perovskite films exhibited excellent water resistance under an ambient environment with a RH of 60 ± 5% for 100 h. Furthermore, it could even resist direct contact with water for 60 s without significant degradation. Under these circumstances, PEAX-treated perovskite film-based PeSCs exhibited long-term stability. The PeSCs with PEAI and PEABr maintained more than 76.5 and 82.8%, respectively, of their original PCE under an ambient environment with a RH of 30 ± 5% over 500 h, which was much higher than that (25.6%) of the control device. Even under a high RH of 60 ± 5%, PeSCs modified by PEAI and PEABr still held 80.5 and 85.2% of the original PCE after exposure for 100 h, respectively. However, the control device rapidly lost over 99% of the initial PCE after only 60 h. Except for the long-term stability, the PCE of the PeSC devices also improved after decoration with PEAX. The control device exhibited a relatively low PCE of 13.28%. In contrast, the champion PCEs of the devices with PEAI and PEABr reached 17.33 and 17.18%, respectively. Because the fabrication process of our blending method with PEAX is much simpler and easier to employ than other passivation methods, we believe this work could have a significant impact on the transition of PeSCs into real-world applications.

■ ASSOCIATED CONTENT

Supporting Information

The Supporting Information is available free of charge at https://pubs.acs.org/doi/10.1021/acsami.1c09093.

SEM images of perovskite films with 5 mg/mL PEAI and PEABr and corresponding elemental distributions, cross-sectional diagrams of films, XRD and high-resolution XRD patterns of perovskite films with different concentrations of PEABr, SEM images of perovskite films with different concentrations of PEABr, high-resolution XPS spectrum of Br 3d energy level, water-contact-angle of perovskite films, color of control film after exposure for 5 h, schematic structure of the PeSC device, $J-V$ curves of the solar cell devices with various dopant concentrations, device parameters of devices with different PEAI and PEABr concentrations, element contents of PEABr-modified perovskite film from XPS measurement, different types of iodine atoms in $MAPbI_3$ unit cell, schematic diagram of $MAPbI_3$ super cell, atomic parameters of iodine atoms in $MAPbI_3$ unit cell, crystalline structures, calculated band structures and partial density of states of pristine $MAPbI_3$ and $MAPbI_{3-x}Br_x$, UPS spectra of perovskite films w/o and with PEABr, UV−visible absorption spectra of perovskite films with and without PEABr, and photo of device with Al electrodes stored under ambient environment for 500 h (PDF)

Demonstration of the strong stability of films induced by PEAX (MP4)

■ AUTHOR INFORMATION

Corresponding Authors

Kwang Ho Kim − *Hybrid Interface Materials Global Frontier Research Group, Pusan National University, Busan 608-737, Republic of Korea*; Email: kwhkim@pusan.ac.kr

Sung Heum Park − *Department of Physics, Pukyong National University, Busan 48513, Republic of Korea; Hybrid Interface Materials Global Frontier Research Group, Pusan National University, Busan 608-737, Republic of Korea*; orcid.org/0000-0001-5701-660X; Email: spark@pknu.ac.kr

Authors

Yuanyuan Zhang − *Department of Physics, Pukyong National University, Busan 48513, Republic of Korea; Hybrid Interface Materials Global Frontier Research Group, Pusan National University, Busan 608-737, Republic of Korea*

Qiao Chen − *Department of Chemistry and Pharmaceutical Science, Qingdao Agricultural University, Qingdao 266109, PR China*

Hyun-Seock Yang − *Department of Physics, Pukyong National University, Busan 48513, Republic of Korea; Hybrid Interface Materials Global Frontier Research Group, Pusan National University, Busan 608-737, Republic of Korea*

Danbi Kim − *Department of Physics, Pukyong National University, Busan 48513, Republic of Korea; Hybrid Interface Materials Global Frontier Research Group, Pusan National University, Busan 608-737, Republic of Korea*

Insoo Shin − *Department of Physics, Pukyong National University, Busan 48513, Republic of Korea*

Bo Ram Lee − *Department of Physics, Pukyong National University, Busan 48513, Republic of Korea*; orcid.org/0000-0002-4670-6717

Joo Hyun Kim − *Department of Polymer Engineering, Pukyong National University, Busan 48513, Republic of Korea*; orcid.org/0000-0002-1507-1640

Doo Kyung Moon − *Department of Chemical Engineering, Konkuk University, Seoul 05029, Republic of Korea*; orcid.org/0000-0001-9482-7508

Complete contact information is available at: https://pubs.acs.org/10.1021/acsami.1c09093

Notes

The authors declare no competing financial interest.

https://doi.org/10.1021/acsami.1c09093
ACS Appl. Mater. Interfaces 2021, 13, 33172−33181

■ ACKNOWLEDGMENTS

The research was mainly supported by the Global Frontier Program through the Global Frontier Hybrid Interface Materials (GFHIM) of the National Research Foundation of Korea (NRF) funded by the Ministry of Science, ICT & Future Planning (2013M3A6 B1078874). The research was also supported by the New & Renewable Energy Core Technology Program of the Korea Institute of Energy Technology Evaluation and Planning (KETEP) granted financial resource from the Ministry of Trade, Industry & Energy, Republic of Korea (20193091010110). This research was also supported by the Nano Material Technology Development Program through NRF funded by the Ministry of Science and ICT (2021M3H4A1A02057007).

■ REFERENCES

(1) Jeon, N. J.; Na, H.; Jung, E. H.; Yang, T.-Y.; Lee, Y. G.; Kim, G.; Shin, H.-W.; Il Seok, S.; Lee, J.; Seo, J. A Fluorene-Terminated Hole-Transporting Material for Highly Efficient and Stable Perovskite Solar Cells. *Nat. Energy* **2018**, *3*, 682−689.

(2) Wang, K.; Tang, M. C.; Dang, H. X.; Munir, R.; Barrit, D.; De Bastiani, M.; Aydin, E.; Smilgies, D. M.; Wolf, S.; Amassian, A. Kinetic Stabilization of the Sol−Gel State in Perovskites Enables Facile Processing of High-Efficiency Solar Cells. *Adv. Mater.* **2019**, *31*, 1808357.

(3) Huang, H.-H.; Shih, Y.-C.; Wang, L.; Lin, K.-F. Boosting the Ultra-Stable Unencapsulated Perovskite Solar Cells by Using Montmorillonite/$CH_3NH_3PbI_3$ Nanocomposite as Photoactive Layer. *Energy Environ. Sci.* **2019**, *12*, 1265−1273.

(4) Jiang, Q.; Zhao, Y.; Zhang, X.; Yang, X.; Chen, Y.; Chu, Z.; Ye, Q.; Li, X.; Yin, Z.; You, J. Surface Passivation of Perovskite Film for Efficient Solar Cells. *Nat. Photonics* **2019**, *13*, 460−466.

(5) Matsui, T.; Yamamoto, T.; Nishihara, T.; Morisawa, R.; Yokoyama, T.; Sekiguchi, T.; Negami, T. Compositional Engineering for Thermally Stable, Highly Efficient Perovskite Solar Cells Exceeding 20% Power Conversion Efficiency with 85 °C/85% 1000 h Stability. *Adv. Mater.* **2019**, *31*, No. e1806823.

(6) Gao, L.; Spanopoulos, I.; Ke, W.; Huang, S.; Hadar, I.; Chen, L.; Li, X.; Yang, G.; Kanatzidis, M. G. Improved Environmental Stability and Solar Cell Efficiency of (MA,FA)PbI_3 Perovskite Using a Wide-Band-Gap 1D Thiazolium Lead Iodide Capping Layer Strategy. *ACS Energy Lett.* **2019**, *4*, 1763−1769.

(7) Lin, Y.; Fang, Y.; Zhao, J.; Shao, Y.; Stuard, S. J.; Nahid, M. M.; Ade, H.; Wang, Q.; Shield, J. E.; Zhou, N.; Moran, A. M.; Huang, J. Unveiling the Operation Mechanism of Layered Perovskite Solar Cells. *Nat. Commun.* **2019**, *10*, 1008.

(8) Wu, C.; Wang, K.; Feng, X.; Jiang, Y.; Yang, D.; Hou, Y.; Yan, Y.; Sanghadasa, M.; Priya, S. Ultrahigh Durability Perovskite Solar Cells. *Nano Lett.* **2019**, *19*, 1251−1259.

(9) Zheng, X.; Troughton, J.; Gasparini, N.; Lin, Y.; Wei, M.; Hou, Y.; Liu, J.; Song, K.; Chen, Z.; Yang, C.; Turedi, B.; Alsalloum, A. Y.; Pan, J.; Chen, J.; Zhumekenov, A. A.; Anthopoulos, T. D.; Han, Y.; Baran, D.; Mohammed, O. F.; Sargent, E. H.; Bakr, O. M. Quantum Dots Supply Bulk- and Surface-Passivation Agents for Efficient and Stable Perovskite Solar Cells. *Joule* **2019**, *3*, 1963−1976.

(10) You, S.; Wang, H.; Bi, S.; Zhou, J.; Qin, L.; Qiu, X.; Zhao, Z.; Xu, Y.; Zhang, Y.; Shi, X.; Zhou, H.; Tang, Z. A Biopolymer Heparin Sodium Interlayer Anchoring TiO_2 and $MAPbI_3$ Enhances Trap Passivation and Device Stability in Perovskite Solar Cells. *Adv. Mater.* **2018**, *30*, No. e1706924.

(11) Li, X.; Zhang, W.; Wang, Y.-C.; Zhang, W.; Wang, H.-Q.; Fang, J. In-Situ Cross-Linking Strategy for Efficient and Operationally Stable Methylammoniun Lead Iodide Solar Cells. *Nat. Commun.* **2018**, *9*, 3806.

(12) Chen, J.; Zuo, L.; Zhang, Y.; Lian, X.; Fu, W.; Yan, J.; Li, J.; Wu, G.; Li, C.-Z.; Chen, H. High-Performance Thickness Insensitive Perovskite Solar Cells with Enhanced Moisture Stability. *Adv. Energy Mater.* **2018**, *8*, 1800438.

(13) Jung, M.; Shin, T. J.; Seo, J.; Kim, G.; Seok, S. I. Structural Features and Their Functions in Surfactant-Armoured Methylammonium Lead Iodide Perovskites for Highly Efficient and Stable Solar Cells. *Energy Environ. Sci.* **2018**, *11*, 2188−2197.

(14) Jeon, I.; Shawky, A.; Lin, H.-S.; Seo, S.; Okada, H.; Lee, J.-W.; Pal, A.; Tan, S.; Anisimov, A.; Kauppinen, E. I.; Yang, Y.; Manzhos, S.; Maruyama, S.; Matsuo, Y. Controlled Redox of Lithium-Ion Endohedral Fullerene for Efficient and Stable Metal Electrode-Free Perovskite Solar Cells. *J. Am. Chem. Soc.* **2019**, *141*, 16553−16558.

(15) Wu, S.; Chen, R.; Zhang, S.; Babu, B. H.; Yue, Y.; Zhu, H.; Yang, Z.; Chen, C.; Chen, W.; Huang, Y.; Fang, S.; Liu, T.; Han, L.; Chen, W. A Chemically Inert Bismuth Interlayer Enhances Long-Term Stability of Inverted Perovskite Solar Cells. *Nat. Commun.* **2019**, *10*, 1161.

(16) Wu, Z.; Liu, Z.; Hu, Z.; Hawash, Z.; Qiu, L.; Jiang, Y.; Ono, L. K.; Qi, Y. Highly Efficient and Stable Perovskite Solar Cells via Modification of Energy Levels at the Perovskite/Carbon Electrode Interface. *Adv. Mater.* **2019**, *31*, 1804284.

(17) Zhao, Y.; Zhu, P.; Wang, M.; Huang, S.; Zhao, Z.; Tan, S.; Han, T. H.; Lee, J. W.; Huang, T.; Wang, R.; Xue, J.; Meng, D.; Huang, Y.; Marian, J.; Zhu, J.; Yang, Y. A Polymerization-Assisted Grain Growth Strategy for Efficient and Stable Perovskite Solar Cells. *Adv. Mater.* **2020**, *32*, No. e1907769.

(18) Xie, L.; Chen, J.; Vashishtha, P.; Zhao, X.; Shin, G. S.; Mhaisalkar, S. G.; Park, N.-G. Importance of Functional Groups in Cross-Linking Methoxysilane Additives for High-Efficiency and Stable Perovskite Solar Cells. *ACS Energy Lett.* **2019**, *4*, 2192−2200.

(19) Wang, F.; Jiang, X.; Chen, H.; Shang, Y.; Liu, H.; Wei, J.; Zhou, W.; He, H.; Liu, W.; Ning, Z. 2D-Quasi-2D-3D Hierarchy Structure for Tin Perovskite Solar Cells with Enhanced Efficiency and Stability. *Joule* **2018**, *2*, 2732−2743.

(20) Li, P.; Zhang, Y.; Liang, C.; Xing, G.; Liu, X.; Li, F.; Liu, X.; Hu, X.; Shao, G.; Song, Y. Phase Pure 2D Perovskite for High-Performance 2D-3D Heterostructured Perovskite Solar Cells. *Adv. Mater.* **2018**, *30*, No. e1805323.

(21) Lee, D. S.; Yun, J. S.; Kim, J.; Soufiani, A. M.; Chen, S.; Cho, Y.; Deng, X.; Seidel, J.; Lim, S.; Huang, S.; Ho-Baillie, A. W. Y. Passivation of Grain Boundaries by Phenethylammonium in Formamidinium-Methylammonium Lead Halide Perovskite Solar Cells. *ACS Energy Lett.* **2018**, *3*, 647−654.

(22) Lim, J. W.; Wang, H.; Choi, C. H.; Kwon, H.; Quan, L. N.; Park, W.-T.; Noh, Y.-Y.; Kim, D. H. Self-Powered Reduced-Dimensionality Perovskite Photodiodes with Controlled Crystalline Phase and Improved Stability. *Nano Energy* **2019**, *57*, 761−770.

(23) Li, M. H.; Yeh, H. H.; Chiang, Y. H.; Jeng, U. S.; Su, C. J.; Shiu, H. W.; Hsu, Y. J.; Kosugi, N.; Ohigashi, T.; Chen, Y. A.; Shen, P. S.; Chen, P.; Guo, T. F. Highly Efficient 2D/3D Hybrid Perovskite Solar Cells via Low-Pressure Vapor-Assisted Solution Process. *Adv. Mater.* **2018**, *30*, No. e1801401.

(24) Zhou, L.; Lin, Z.; Ning, Z.; Li, T.; Guo, X.; Ma, J.; Su, J.; Zhang, C.; Zhang, J.; Liu, S.; Chang, J.; Hao, Y. Highly Efficient and Stable Planar Perovskite Solar Cells with Modulated Diffusion Passivation Toward High Power Conversion Efficiency and Ultrahigh Fill Factor. *Sol. RRL* **2019**, *3*, 1900293.

(25) Liu, Y.; Duan, J.; Zhang, J.; Huang, S.; Ou-Yang, W.; Bao, Q.; Sun, Z.; Chen, X. High Efficiency and Stability of Inverted Perovskite Solar Cells Using Phenethyl Ammonium Iodide-Modified Interface of NiOx and Perovskite Layers. *ACS Appl. Mater. Interfaces* **2020**, *12*, 771−779.

(26) Wang, H.; Bian, H.; Jin, Z.; Liang, L.; Bai, D.; Wang, Q.; Liu, S. F. Synergy of Hydrophobic Surface Capping and Lattice Contraction for Stable and High-Efficiency Inorganic $CsPbI_2Br$ Perovskite Solar Cells. *Sol. RRL* **2018**, *2*, 1800216.

(27) Liu, Y.; Shin, I.; Hwang, I.-W.; Kim, S.; Lee, J.; Yang, M.-S.; Jung, Y. K.; Jang, J.-W.; Jeong, J. H.; Park, S. H.; Kim, K. H. Single-Crystal-like Perovskite for High-Performance Solar Cells Using the Effective Merged Annealing Method. *ACS Appl. Mater. Interfaces* **2017**, *9*, 12382−12390.

https://doi.org/10.1021/acsami.1c09093
ACS Appl. Mater. Interfaces 2021, 13, 33172−33181

(28) Hohenberg, P.; Kohn, W. Inhomogeneous Electron Gas. *Phys. Rev.* **1964**, *136*, B864−B871.
(29) Kohn, W.; Sham, L. J. Self-Consistent Equations Including Exchange and Correlation Effects. *Phys. Rev.* **1965**, *140*, A1133−A1138.
(30) Payne, M. C.; Teter, M. P.; Allan, D. C.; Arias, T. A.; Joannopoulos, J. D. Iterative Minimization Techniques for AB Initio Total-Energy Calculations: Molecular Dynamics and Conjugate Gradients. *Rev. Mod. Phys.* **1992**, *64*, 1045−1097.
(31) Zhang, Y.; Jang, S.; Hwang, I.-W.; Jung, Y. K.; Lee, B. R.; Kim, J. H.; Kim, K. H.; Park, S. H. Bilateral Interface Engineering for Efficient and Stable Perovskite Solar Cells Using Phenylethylammonium Iodide. *ACS Appl. Mater. Interfaces* **2020**, *12*, 24827−24836.
(32) Duan, B.; Ren, Y.; Xu, Y.; Chen, W.; Ye, Q.; Huang, Y.; Zhu, J.; Dai, S. Identification and Characterization of A New Intermediate to Obtain High Quality Perovskite Films with Hydrogen Halides as Additives. *Inorg. Chem. Front.* **2017**, *4*, 473−480.
(33) Ma, Y.; Liu, Y.; Shin, I.; Hwang, I.-W.; Jung, Y. K.; Jeong, J. H.; Park, S. H.; Kim, K. H. Understanding and Tailoring Grain Growth of Lead-Halide Perovskite for Solar Cell Application. *ACS Appl. Mater. Interfaces* **2017**, *9*, 33925−33933.
(34) Ren, Y.; Chen, J.; Ji, D.; Sun, Y.; Li, C. Improve the Quality of $HC(NH_2)_2PbI_xBr_{3-x}$ Through Iodine Vacancy Filling for Stable Mixed Perovskite Solar Cells. *Chem. Eng. J.* **2019**, *384*, 123273.
(35) Conings, B.; Baeten, L.; De Dobbelaere, C.; D'Haen, J.; Manca, J.; Boyen, H.-G. Perovskite-Based Hybrid Solar Cells Exceeding 10% Efficiency with High Reproducibility Using a Thin Film Sandwich Approach. *Adv. Mater.* **2014**, *26*, 2041−2046.
(36) Lenczewska, K.; Gerasymchuk, Y.; Vu, N.; Liem, N. Q.; Boulon, G.; Hreniak, D. The Size Effect on the Energy Transfer in Bi^{3+}−Eu^{3+} Co-Doped $GdVO_4$ Nanocrystals. *J. Mater. Chem. C* **2017**, *5*, 3014−3023.
(37) Wang, H.; Zhu, C.; Liu, L.; Ma, S.; Liu, P.; Wu, J.; Shi, C.; Du, Q.; Hao, Y.; Xiang, S.; Chen, H.; Chen, P.; Bai, Y.; Zhou, H.; Li, Y.; Chen, Q. Interfacial Residual Stress Relaxation in Perovskite Solar Cells with Improved Stability. *Adv. Mater.* **2019**, *31*, 1904408.
(38) Zeng, L.; Chen, Z.; Qiu, S.; Hu, J.; Li, C.; Liu, X.; Liang, G.; Brabec, C. J.; Mai, Y.; Guo, F. 2D-3D Heterostructure Enables Scalable Coating of Efficient Low-BandGap Sn−Pb Mixed Perovskite Solar Cells. *Nano Energy* **2019**, *66*, 104099.
(39) Shao, Z.; Wang, Z.; Li, Z.; Fan, Y.; Meng, H.; Liu, R.; Wang, Y.; Hagfeldt, A.; Cui, G.; Pang, S. A Scalable Methylamine Gas Healing Strategy for High-Efficiency Inorganic Perovskite Solar Cells. *Angew. Chem., Int. Ed.* **2019**, *58*, 5587−5591.
(40) Yang, M.; Li, Z.; Reese, M. O.; Reid, O. G.; Kim, D. H.; Siol, S.; Klein, T. R.; Yan, Y.; Berry, J. J.; van Hest, M. F. A. M.; Zhu, K. Perovskite Ink with Wide Processing Window for Scalable High-Efficiency Solar Cells. *Nat. Energy* **2017**, *2*, 17038.
(41) Tsai, H.; Nie, W.; Blancon, J.-C.; Stoumpos, C. C.; Asadpour, R.; Harutyunyan, B.; Neukirch, A. J.; Verduzco, R.; Crochet, J. J.; Tretiak, S.; Pedesseau, L.; Even, J.; Alam, M. A.; Gupta, G.; Lou, J.; Ajayan, P. M.; Bedzyk, M. J.; Kanatzidis, M. G.; Mohite, A. D. High-Efficiency Two-Dimensional Ruddlesden−Popper Perovskite Solar Cells. *Nature* **2016**, *536*, 312−316.
(42) Wang, Q.; Mosconi, E.; Wolff, C.; Li, J.; Neher, D.; De Angelis, F.; Suranna, G. P.; Grisorio, R.; Abate, A. Rationalizing the Molecular Design of Hole-Selective Contacts to Improve Charge Extraction in Perovskite Solar Cells. *Adv. Energy Mater.* **2019**, *9*, 1900990.
(43) Brenner, T. M.; Egger, D. A.; Kronik, L.; Hodes, G.; Cahen, D. Hybrid Organic—Inorganic Perovskites: Low-Cost Semiconductors with Intriguing Charge-Transport Properties. *Nat. Rev. Mater.* **2016**, *1*, 15007.
(44) Guerrero, A.; You, J.; Aranda, C.; Kang, Y. S.; Garcia-Belmonte, G.; Zhou, H.; Bisquert, J.; Yang, Y. Interfacial Degradation of Planar Lead Halide Perovskite Solar Cells. *ACS Nano* **2016**, *10*, 218−224.
(45) Azmi, R.; Hadmojo, W. T.; Sinaga, S.; Lee, C.-L.; Yoon, S. C.; Jung, I. H.; Jang, S.-Y. High-Efficiency Low-Temperature ZnO Based Perovskite Solar Cells Based on Highly Polar, Nonwetting Self-Assembled Molecular Layers. *Adv. Energy Mater.* **2018**, *8*, 1701683.
(46) Stolterfoht, M.; Wolff, C. M.; Márquez, J. A.; Zhang, S.; Hages, C. J.; Rothhardt, D.; Albrecht, S.; Burn, P. L.; Meredith, P.; Unold, T.; Neher, D. Visualization and Suppression of Interfacial Recombination for High-Efficiency Large-Area Pin Perovskite Solar Cells. *Nat. Energy* **2018**, *3*, 847−854.
(47) Lu, J.; Lin, X.; Jiao, X.; Gengenbach, T.; Scully, A. D.; Jiang, L.; Tan, B.; Sun, J.; Li, B.; Pai, N.; Bach, U.; Simonov, A. N.; Cheng, Y.-B. Interfacial Benzenethiol Modification Facilitates Charge Transfer and Improves Stability of cm-Sized Metal Halide Perovskite Solar Cells with up to 20% Efficiency. *Energy Environ. Sci.* **2018**, *11*, 1880−1889.
(48) Duan, J.; Zhao, Y.; Wang, Y.; Yang, X.; Tang, Q. Hole-Boosted $Cu(Cr,M)O_2$ Nanocrystals for All-Inorganic $CsPbBr_3$ Perovskite Solar Cells. *Angew. Chem., Int. Ed.* **2019**, *58*, 16147−16151.
(49) Duan, J.; Zhao, Y.; He, B.; Tang, Q. High-Purity Inorganic Perovskite Films for Solar Cells with 9.72% Efficiency. *Angew. Chem., Int. Ed.* **2018**, *57*, 3787−3791.
(50) Tan, H.; Jain, A.; Voznyy, O.; Lan, X.; García de Arquer, F. P.; Fan, J. Z.; Quintero-Bermudez, R.; Yuan, M.; Zhang, B.; Zhao, Y.; Fan, F.; Li, P.; Quan, L. N.; Zhao, Y.; Lu, Z.-H.; Yang, Z.; Hoogland, S.; Sargent, E. H. Efficient and Stable Solution-Processed Planar Perovskite Solar Cells via Contact Passivation. *Science* **2017**, *355*, 722−726.
(51) Li, H.; Shi, W.; Huang, W.; Yao, E.-P.; Han, J.; Chen, Z.; Liu, S.; Shen, Y.; Wang, M.; Yang, Y. Carbon Quantum Dots/TiO_x Electron Transport Layer Boosts Efficiency of Planar Heterojunction Perovskite Solar Cells to 19%. *Nano Lett.* **2017**, *17*, 2328−2335.
(52) Emara, J.; Schnier, T.; Pourdavoud, N.; Riedl, T.; Meerholz, K.; Olthof, S. Impact of Film Stoichiometry on the Ionization Energy and Electronic Structure of $CH_3NH_3PbI_3$ Perovskites. *Adv. Mater.* **2016**, *28*, 553−559.
(53) Hao, F.; Stoumpos, C. C.; Cao, D. H.; Chang, R. P. H.; Kanatzidis, M. G. Lead-Free Solid-State Organic−Inorganic Halide Perovskite Solar Cells. *Nat. Photonics* **2014**, *8*, 489−494.
(54) Kim, M.-c.; Kim, B. J.; Son, D.-Y.; Park, N.-G.; Jung, H. S.; Choi, M. Observation of Enhanced Hole Extraction in Br Concentration Gradient Perovskite Materials. *Nano Lett.* **2016**, *16*, 5756−5763.
(55) Chen, L.; Tan, Y.-Y.; Chen, Z.-X.; Wang, T.; Hu, S.; Nan, Z.-A.; Xie, L.-Q.; Hui, Y.; Huang, J.-X.; Zhan, C.; Wang, S.-H.; Zhou, J.-Z.; Yan, J.-W.; Mao, B.-W.; Tian, Z.-Q. Toward Long-Term Stability: Single-Crystal Alloys of Cesium-Containing Mixed Cation and Mixed Halide Perovskite. *J. Am. Chem. Soc.* **2019**, *141*, 1665−1671.
(56) Hangoma, P. M.; Ma, Y.; Shin, I.; Liu, Y.; Park, W. I.; Jung, Y. K.; Lee, B. R.; Jeong, J. H.; Park, S. H.; Kim, K. H. Improved Moisture Stability of Perovskite Solar Cells with a Surface-Treated PCBM Layer. *Sol. RRL* **2019**, *3*, 1800289.

https://doi.org/10.1021/acsami.1c09093
ACS Appl. Mater. Interfaces 2021, 13, 33172−33181